# Microscale thermo-elastic analysis of composite materials by high-order geometrically accurate finite elements

(Article begins on next page)

07 May 2024

# Microscale thermo-elastic analysis of composite materials by high-order geometrically accurate finite elements

A.R. Sánchez-Majano [a], R. Masia [a], A. Pagani [a,*], E. Carrera [a,b]

[a] *Mul2 Lab, Department of Mechanical and Aerospace Engineering, Politecnico di Torino, Corso Duca degli Abruzzi 24, 10129 Torino, Italy*
[b] *Department of Mechanical Engineering, College of Engineering, Prince Mohammad Bin Fahd University, Kingdom of Saudi Arabia*

## ABSTRACT

The present work proposes a new approach for conducting thermo-elastic micromechanical analysis. It relies on the use of high-order and geometrically accurate beam finite elements to model the microstructures. The governing equations of the micromechanics models involving the unit cell concept are derived through the Mechanics of Structure Genome (MSG). MSG allows multiscale analysis where global and local scales are decoupled and provides the constitutive information and local fields without needing ad hoc assumptions or requiring different loading steps. The high-order beam elements are derived instead by means of the well-known Carrera Unified Formulation (CUF). These advanced models provide a level of accuracy comparable to conventional solid elements with a fraction of the computational effort. Depending on the problem considered, the cross-section of the refined beam model is modelled by a set of Legendre polynomials, whilst the main direction of the representative unit cell is discretised using one-dimensional (1D) finite elements. Additionally, a non-isoparametric mapping technique allows a perfect description of the microstructural constituents. The present approach enables the resolution of both thermo-elastic homogenisation problems and the recovery of local stress fields through a single run of a CUF-MSG-based code. Several numerical examples compared with numerous other representative solutions of fibre and particle reinforced composites are conducted in order to demonstrate the validity and the efficiency of the presented methodology.

## 1. Introduction

In recent decades, many research fields have considered the phenomena that occur at the different scales of their problems of interest. As a result, the locution *multiscale modelling* has been widely extended and become a trend. Notably, the contributions in material modelling have been noteworthy. The quintessence of multiscale approaches resides in deriving equations, parameters, or simulation algorithms that provide information about the behaviour at a given length scale on the basis of the physics at an inner scale, assuming that the inner scale physics are better understood than those at the outer scales.

Aerospace is an engineering field in which the structures are conformed by hierarchical materials, such as composite materials, where the finer scales play a pivotal role in the overall structural behaviour. However, the main difficulty when using composites is the inability to perform direct numerical simulations due to the enormous computational cost it would require. Hence, multiscale modelling paves the way to treat this sort of numerical problem, in which a multi-step approach is taken to solve the problem, taking into account the different length scales. Through this method, all the analyses are linked from the constituent level to the whole operating structure, thus creating a bottom-up flow of information, as presented in Llorca et al. [1]. In this context, the microstructural problem is solved by computational micromechanics to obtain accurate constitutive models useful for the structural study at the mesoscale level, for example, at the laminate level, as stated in [2,3].

Micromechanical modelling methods represent helpful tools to predict the way the presence of voids, the arrangement of the fibre, the fibre fraction, or the constituents' geometry influence the overall response of the homogenised equivalent material. Many numerical, analytical and semi-analytical methods have been developed in recent decades, proving the continuous evolution of this research field. Insightful reviews on micromechanical modelling can be found in [4–6]. Many of these methods assume that the fibres are arranged following a periodic pattern, recalling the Repeating Unit Cell (RUC) concept, already described in detail in the previous work of de Miguel et al. [7]. Some of these methods involve analytical formulae to deal

---

with the RUC problem, for instance, the rule of mixtures [8], Rosen and Hashin [9] upper and lower bounds, the Hashin and Shtrikman [10], the elasticity-based cell method [11], or the Mori–Tanaka method [12]. In contrast, other authors provide more advanced solutions, such as the Method of Cells (MOC) [13], the Generalised Method of Cells (GMC) [14] and the High-Fidelity Method of Cells (HFGMC) [15], which are suitable for more general cases. Another widely spread methodology consists in applying suitable boundary tractions or boundary displacements to a Representative Volume Element (RVE) and subsequently performing conventional stress analyses to calculate the elastic properties as proposed in [16]. Finally, recent works use experiments and commercial software like ABAQUS to derive the homogenised features of RVE models, as in [17].

In this article, the RUC problem is solved by coupling the Mechanics of Structure Genome (MSG), proposed in [18] by Yu, with a novel one-dimensional (1D) approach. Yu established the concept of Structure Genome (SG), which is defined as the fundamental building block containing the mathematical features of every structure. For example, the SG can be seen as a 3D repeating body of microstructures featuring variations of the phases over the three-dimensional space. The Variational Asymptotic Method (VAM) [19] is the basis of the MSG method and allows problems involving smaller parameters to be solved. This characteristic makes the VAM method highly suitable for solving problems involving composite. Indeed, VAM is employed to compute the homogenised properties and local solutions of periodically heterogeneous materials through an asymptotic approach for the RUC problem with a high level of efficiency and accuracy [20,21].

As stated earlier, this work proposes a 1D model to solve these demanding computational models by means of the well-known Carrera Unified Formulation (CUF) [22], which allows reducing general 3D problems into less demanding 1D [23,24] and 2D [25,26] models, while still providing highly accurate solutions. In this regard, arbitrary expansion functions can be employed to characterise the cross-section and through-the-thickness direction for 1D and 2D problems, respectively, and obtain numerical models that overcome the limitations of classical structural theories. Profiting from these capabilities, the RUC can be modelled using 1D models along the fibre or inclusion direction. Then, Hierarchical Legendre Expansion (HLE) [27] is used to describe the geometry of the constituents by coupling it with blending functions in order to obtain a high-order non-isoparametric numerical model [28]. Finally, the validity and accuracy of the proposed refined beam modelling to solve the thermo-elastic micromechanical MSG problem are demonstrated. Note that the pure elastic micromechanical problem was already addressed in the work of de Miguel et al. [7] and that an extension to the thermo-elastic case is proven by adding the computation of the effective coefficient of thermal expansion and by considering the temperature change in the retrieval of the local stresses.

The document is organised as follows: first, the application of VAM to the unit cell is presented in Section 2; then, the CUF models that are used to solve the MSG problem are introduced in Section 3, while its application to the homogenisation and dehomogenisation of different RUC geometries is available in 4. Lastly, conclusions are drawn in Section 5.

## 2. Variational asymptotic method for the thermo-elastic unit cell problem

The fundamental idea behind micromechanical analyses is that the size of the RUC is significantly smaller than the dimension of the global structure, such that $\mathbf{y} = \mathbf{x}/\delta$, with $\delta$ small scaling parameter that characterises the size of the RUC, and $\mathbf{y}$ and $\mathbf{x}$ are the local and global reference systems of the RUC, respectively. Another assumption is that the geometry, the different loading conditions and the boundary conditions concerning the macroscale problem do not affect the effective material properties provided by RUC analysis at the microscale. Additionally, the local solutions have an average value over the RUC
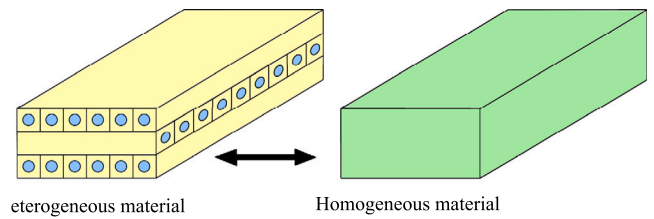


**Fig. 1.** Representation of heterogeneous and homogenised material. The former accounts for the fibre and matrix material properties, whilst the latter uses the effective material properties.

volume corresponding to the global solution of the macroscopic problem. Applying this to the displacement field $\mathbf{u}(\mathbf{x};\mathbf{y})$, this assumption reads as:

$$\bar{\mathbf{u}}(\mathbf{x}) = \frac{1}{V}\int_V \mathbf{u}(\mathbf{x};\mathbf{y})dV \tag{1}$$

where $\bar{\mathbf{u}}(\mathbf{x})$ represents the averaged displacements vector, which only depends on the global coordinates, $\mathbf{u}(\mathbf{x};\mathbf{y})$ is the local field of displacements that depends on both the global and the local coordinates, and $V$ denotes the total volume of the cell. Furthermore, to guarantee the compatibility of deformations concerning the neighbouring RUCs, periodic boundary conditions are applied and can be expressed as:

$$u_i(x_1, x_2, x_3; L_1/2, y_2, y_3) = u_i(x_1 + L_1, x_2, x_3; -L_1/2, y_2, y_3) \tag{2}$$
$$u_i(x_1, x_2, x_3; y_1, 0, y_3) = u_i(x_1, x_2 + L_2, x_3; y_1, L_2, y_3)$$
$$u_i(x_1, x_2, x_3; y_1, y_2, L_3/2) = u_i(x_1, x_2, x_3 + L_3; y_1, y_2, -L_3/2)$$

where $L_i$ denotes the characteristic dimension of the RUC in the $y_i$ direction as depicted in Fig. 2.

According to the MSG, by minimising the difference between the strain energies of the heterogeneous material and the homogenised material, one can compute the solution to the stationary value problem (see Fig. 1) [20], expressed in the following functional:

$$\Pi = \frac{1}{2}\left\langle C_{ijkl}\varepsilon_{ij}\varepsilon_{kl} + 2\beta_{ij}\varepsilon_{ij}\theta + c_v\frac{\theta^2}{T_0}\right\rangle$$
$$- \frac{1}{2}\left(C_{ijkl}^*\bar{\varepsilon}_{ij}\bar{\varepsilon}_{kl} + 2\beta_{ij}^*\bar{\varepsilon}_{ij}\theta + c_v^*\frac{\theta^2}{T_0}\right) \tag{3}$$

where the first term is the strain energy of the heterogeneous composite represented by the RUC, whilst the second one is that of the equivalent homogenised material, and $\langle\rangle$ denotes the volume average. $C_{ijkl}$, $\varepsilon_{ij}$ and $\beta_{ij}$ are the fourth-order elastic tensor, the second-order strain and thermal stress tensors, respectively. $T_0$ is the reference temperature at which the stress-free condition occurs, $c_v$ is the specific heat per unit volume at constant volume, and $\theta$ represents the difference between the current temperature and $T_0$. Note that a constant temperature field is assumed over the RUC volume and that no thermal conductivity effects are accounted for.

To avoid solving the stationary problem for every point in the global system $\mathbf{x}$, it is helpful to formulate the variational statement posed over a single RUC. Hence, the exact solution $\mathbf{u}$ can be expressed by the sum of the global displacements $\bar{\mathbf{u}}$ plus the difference as written below:

$$\mathbf{u}(\mathbf{x};\mathbf{y}) = \bar{\mathbf{u}}(\mathbf{x}) + \delta\chi(\mathbf{x};\mathbf{y}) \tag{4}$$

where $\chi$ represents the fluctuation functions about the global displacements and is scaled down through the use of $\delta$.

The difference in the coordinate systems that play a role in the multiscale problem obliges to calculate the derivatives of a field of the type $\mathbf{u}(\mathbf{x};\mathbf{y})$ as:

$$\frac{\partial\mathbf{u}}{\partial x_j} + \frac{1}{\delta}\frac{\partial\mathbf{u}}{\partial y_j} \tag{5}$$

Hence, applying Eq. (5) to the derivatives of Eq. (4), the strain variables can be expressed as:

$$\varepsilon_{ij}(\mathbf{x};\mathbf{y}) = \bar{\varepsilon}_{ij}(\mathbf{x}) + \chi_{(i,j)}(\mathbf{x};\mathbf{y}) \tag{6}$$

in which

$$\bar{\varepsilon}_{ij}(\mathbf{x}) = \frac{1}{2}\left(\frac{\partial \bar{u}_i(\mathbf{x})}{\partial x_j} + \frac{\partial \bar{u}_j(\mathbf{x})}{\partial x_i}\right) \tag{7}$$

and

$$\chi_{(i,j)}(\mathbf{x};\mathbf{y}) = \frac{1}{2}\left(\frac{\partial \chi_i(\mathbf{x};\mathbf{y})}{\partial y_j} + \frac{\partial \chi_j(\mathbf{x};\mathbf{y})}{\partial y_i}\right) \tag{8}$$

According to Eq. (1), it can be written that $\bar{u}_i = \langle u_i \rangle$ and $\bar{\varepsilon}_{ij} = \langle \varepsilon_{ij} \rangle$, which automatically implies that $\langle \chi_i \rangle = 0$ and $\langle \chi_{(i,j)} \rangle = 0$. Then, employing the field of displacements and strain from Eqs. (4) and (6), respectively, and treating the second term of Eq. (3) as a constant, the unknown fluctuation terms can be solved by minimising the following functional:

$$\Pi^* = \frac{1}{2}\left\langle C_{ijkl}\left[\bar{\varepsilon}_{ij} + \chi_{(i,j)}\right]\left[\bar{\varepsilon}_{kl} + \chi_{(k,l)}\right] + 2\beta_{ij}\left[\bar{\varepsilon}_{ij} + \chi_{(i,j)}\right]\theta + c_v\frac{\theta^2}{T_0}\right\rangle \tag{9}$$

In previous MSG-related works for the RUC homogenisation, the problem is formulated to be solved by conventional Finite Element Analyses (FEA), embedded in a general-purpose multiscale constitutive modelling software named SwiftComp [29]. The innovation of this manuscript is to present an efficient manner to solve the thermo-elastic RUC problem using refined and geometrically accurate beam models.

## 3. Refined beam models for the unit cell problem

According to the geometrical characteristics of the microstructure, MSG can be employed to solve a 3D problem with different elements varying over the three directions, such as composites with particle inclusion, or a 2D problem in which the phases vary within the plane, such as fibre-reinforced composites. Fig. 2 introduces the local coordinate system of the RUC using a square-pack microstructure, though several cases can be analysed using this method. The beam axis, of length L, is set to be the fibre direction $y_1$, while the $y_2, y_3$-plane identifies the cross-section of the beam model $\Omega$. This manuscript foresees the usage of CUF-based 1D models to solve the RUC problem by assuming that the fluctuation unknowns ($\chi$) can be expanded over the cross-section by means of arbitrary expansions ($F_\tau$) depending on the cross-sectional coordinates $y_2$ and $y_3$, as follows:

$$\chi(\mathbf{x};y_1,y_2,y_3) = F_\tau(y_2,y_3)\chi_\tau(\mathbf{x};y_1) \quad \tau = 1,\dots,M \tag{10}$$

where $M$ is the number of expansion terms adopted in the kinematic model and $\tau$ denotes summation. The order of the structural model, and hence the accuracy of the solution, can be tuned by a convenient selection of $F_\tau$, as demonstrated in previous works, see [30,31].

An accurate solution to the micromechanical analysis of heterogeneous materials requires some particular characteristics from the 1D theory. For instance, it should consider the kinematics of each component independently to capture the interface discontinuities, as well as a non-local distribution of the degrees of freedom over the cross-section for an adequate application of the boundary conditions of Eq. (9). That being said, Hierarchical Legendre Expansions (HLE) is coupled with the Blending Function Method (BFM) in order to carry out the micromechanical analyses. These terms are deepened in the upcoming sections.

### 3.1. Hierarchical Legendre Expansions (HLE)

HLE beam models, stated by Carrera et al. [27], are used in this manuscript. They take advantage of the hierarchical features of the Legendre-based polynomials to build sets of high-order polynomials that serve as arbitrary functions over the cross-section $F_\tau$. Clearly, the displacement field, and thus the accuracy, is achieved by the addition
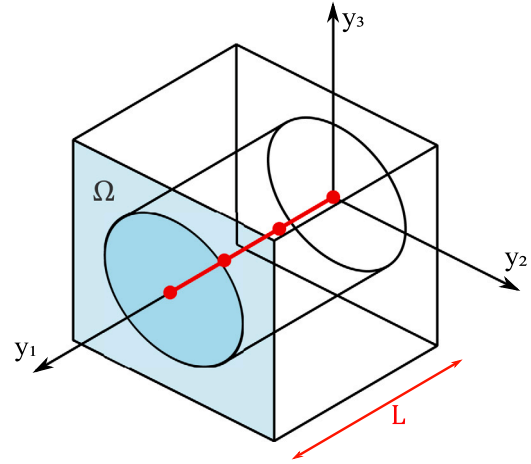


**Fig. 2.** Local coordinate system for RUC problem.

of higher-order polynomials. The available function types are: vertex, side and internal. The vertex functions are defined as:

$$F_\tau = \frac{1}{4}(1 - r_\tau r)(1 - s_\tau s) \qquad \tau = 1,2,3,4 \tag{11}$$

where the value of the terms $r$ and $s$ vary over $-1$ and $1$, and $r_\tau$ e $s_\tau$ represent the vertex coordinates in the natural plane. The vertex expansions correspond to the first-order Lagrange polynomials. Then, an increasing number of side functions are added to the displacement field in order to gain higher-order models:

$$
\begin{aligned}
F_\tau(r,s) &= \frac{1}{2}(1-s)\phi_{p_b}(r) & \tau &= 5,9,13,18,\dots \\
F_\tau(r,s) &= \frac{1}{2}(1+r)\phi_{p_b}(s) & \tau &= 6,10,14,19,\dots \\
F_\tau(r,s) &= \frac{1}{2}(1+s)\phi_{p_b}(r) & \tau &= 7,11,15,20,\dots \\
F_\tau(r,s) &= \frac{1}{2}(1-r)\phi_{p_b}(r) & \tau &= 8,14,16,21,\dots
\end{aligned}
\tag{12}
$$

where $\phi_{p_b}$ corresponds to the 1D internal Legendre-type modes, and $p$ represents the polynomial order of the beam theory. The vertex expansions are defined for $p \geq 2$. Finally, $F_\tau$ internal expansions are defined by multiplying 1D internal modes. When the p-order required is higher than 4, $(p-2)(p-3)/2$ internal functions must be included in the displacement field. Internal functions are defined as follows:

$$
\begin{aligned}
F_{28}(r,s) &= \phi_4(r)\phi_2(s) \\
F_{29}(r,s) &= \phi_3(r)\phi_3(s) \\
F_{30}(r,s) &= \phi_2(r)\phi_4(s)
\end{aligned}
\tag{13}
$$

For further insight on HLE modelling, the reader is invited to read [27,32], where a mathematical description of Legendre polynomials and their application to diverse FEA problems is made.

### 3.2. Cross-section mapping

In order to enable the depiction of generic geometries of the microstructures, the cross-section can be discretised into numerous expansion subdomains. Moreover, various constituents of the RUC problem can be modelled through the compatibility of the displacement at the interfaces of the domains, following a Component Wise (CW) approach [33], where the compatibility of the primary unknowns (fluctuations $\chi$) is imposed at the constituents' interfaces.

Given the high polynomial orders reachable with HLE, keeping the cross-section's domains as large as possible is advantageous. This is fulfilled by adapting the edges of the HLE subdomains to the geometrical characteristics of the different constituents of the microstructures
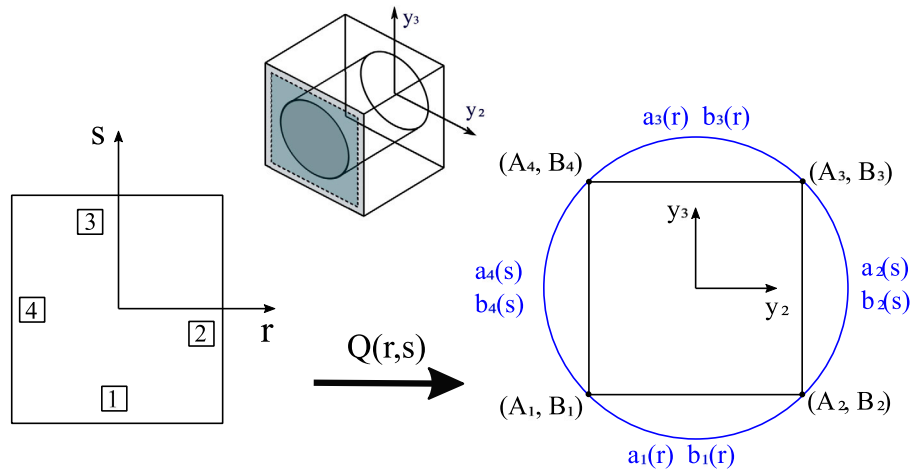
Fig. 3. Mapping technique of the cross-section of the RUC using the blending function.
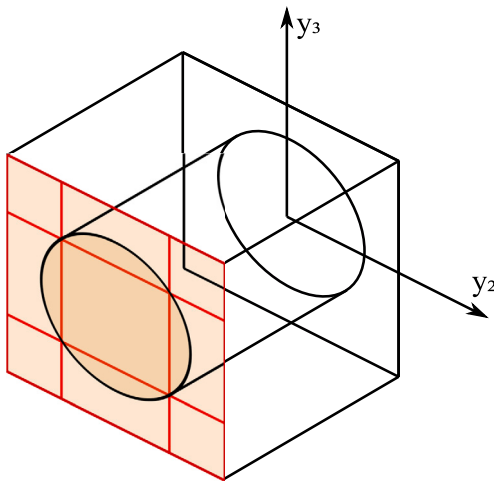


Fig. 4. Expansion domains distributed in the cross-section of fibre-reinforced RUC model. The exact circular geometry is obtained with the blending function capabilities.

using a non-isoparametric mapping technique. Through the use of the blending function, any geometrical description can be parametrised and included in the numerical model [34]. Indeed, this methodology has already been employed in [7,28] to study curved sections that appear in thin-walled structures and in the purely mechanical analysis of multi-phase microstructures, respectively.

In this regard, the blending function method serves to depict the precise geometry of an arbitrary component in the cross-sectional plane $y_2 y_3$. It introduces the mapping functions $\mathbf{Q}$ as follows:

$$
\begin{aligned}
y_2 = Q_a(r,s) &= \frac{1}{2}(1-s)a_1(r) + \frac{1}{2}(1+r)a_2(s) \\
&+ \frac{1}{2}(1+s)a_3(r)\frac{1}{2}(1-r)a_4(s) - F_\tau(r,s)r_\tau \\
y_3 = Q_b(r,s) &= \frac{1}{2}(1-s)b_1(r) + \frac{1}{2}(1+r)b_2(s) \\
&+ \frac{1}{2}(1+s)b_3(r)\frac{1}{2}(1-r)b_4(s) - F_\tau(r,s)s_\tau
\end{aligned}
\tag{14}
$$

where $a_\tau$ and $b_\tau$ are the parametric curves of the borders with $\tau = 1, \ldots, 4$, see Fig. 3. With this procedure, the model's geometry is fixed at the beginning, and the model's accuracy is tuned by only selecting the polynomial order of the structural theory. Hence, there is no need to continuously re-mesh the model to assess the convergence.

### 3.3. Unified high-order finite beam elements

The problem in the beam axis direction $y_1$ can be solved utilising the Finite Element Method (FEM). Throughout this work, the fibre direction is discretised using 1D standard elements. By doing so, the generalised fluctuations unknowns $\chi_\tau(\mathbf{x}; y_1)$ are interpolated with Lagrange shape functions $N_i(y_1)$ on the $y_1$ direction:

$$
\chi_\tau(\mathbf{x}; y_1) = N_i(y_1)\chi_{\tau i}(\mathbf{x}) \quad i = 1, \ldots, N
\tag{15}
$$

where $N$ the total number of beam nodes and $\chi_{\tau i}(\mathbf{x})$ is the nodal unknown vector.

Expressing the global strains in the Voigt notation

$$
\bar{\varepsilon}^T = \left\{ \bar{\varepsilon}_{11} \ \bar{\varepsilon}_{22} \ \bar{\varepsilon}_{33} \ 2\bar{\varepsilon}_{23} \ 2\bar{\varepsilon}_{13} \ 2\bar{\varepsilon}_{12} \right\}
\tag{16}
$$

it is allowed to define the geometrical relations as:

$$
\varepsilon = \bar{\varepsilon} + \mathbf{D}\chi
\tag{17}
$$

with $\mathbf{D}$ as the differential operator. For the sake of brevity, the explicit expression of the differential operator is not included here. Nevertheless, it is available in [7].

Then, Hooke's law relates stresses and strains for the thermo-elastic case as:

$$
\sigma = \mathbf{C}\varepsilon + \beta\theta
\tag{18}
$$

where $\mathbf{C}$ is the $6 \times 6$ material array condensed from the fourth-order tensor $C_{ijkl}$, and $\beta = -\mathbf{C}\alpha$ as the $6 \times 1$ vector condensed matrix from $\beta_{ij}$.

The functional in Eq. (9) can be rewritten as

$$
\Pi^* = \frac{1}{2}\int_V \left[ (\bar{\varepsilon} + \mathbf{D}\chi)^T \mathbf{C}(\bar{\varepsilon} + \mathbf{D}\chi) + 2\beta(\bar{\varepsilon} + \mathbf{D}\chi)\theta + c_v \frac{\theta^2}{T_0} \right] dV
\tag{19}
$$

Periodic boundary conditions of the RUC posing on the sides of the cross-section ($\chi_\tau^+ = \chi_\tau^-$), and on the sections orthogonal to the fibre ($\chi_{\tau 1} = \chi_{\tau n}$) are applied. Then, introducing Eq. (15) in Eq. (10), and the latter into Eq. (19), the functional $\Pi^*$ reads in CUF form as:

$$
\begin{aligned}
\Pi^* = \frac{1}{2}\Big( &\chi_{sj}^T \mathbf{E}^{\tau sij} \chi_{\tau i} + 2\chi_{sj}^T \mathbf{D}_{h\varepsilon}^{sj} \bar{\varepsilon} + \bar{\varepsilon}^T \mathbf{D}_{\varepsilon\varepsilon} \bar{\varepsilon} \\
&+ 2\chi_{sj}^T \mathbf{D}_{h\theta}^{sj}\theta + 2\bar{\varepsilon}^T \mathbf{D}_{\varepsilon\theta}\theta + D_{\theta\theta}\frac{\theta^2}{T_0} \Big)
\end{aligned}
\tag{20}
$$

where

$$
\mathbf{E}^{\tau sij} = \int_\Omega \int_l (\mathbf{D}(F_s N_j \mathbf{I}))^T \mathbf{C}\, \mathbf{D}(F_\tau N_i \mathbf{I}) d\Omega dy_1 \quad \mathbf{D}_{h\varepsilon}^{sj} = \int_\Omega \int_l (\mathbf{D}(F_s N_j \mathbf{I}))^T \mathbf{C} d\Omega dy_1
$$

$$
\mathbf{D}_{\varepsilon\varepsilon} = \int_V \mathbf{C} dV
\tag{21}
$$

$$
\mathbf{D}_{h\theta}^{sj} = \int_\Omega \int_l (\mathbf{D}(F_s N_j \mathbf{I}))^T \beta d\Omega dy_1 \qquad \mathbf{D}_{\varepsilon\theta} = \int_V \beta dV \qquad D_{\theta\theta} = \int_V c_v dV
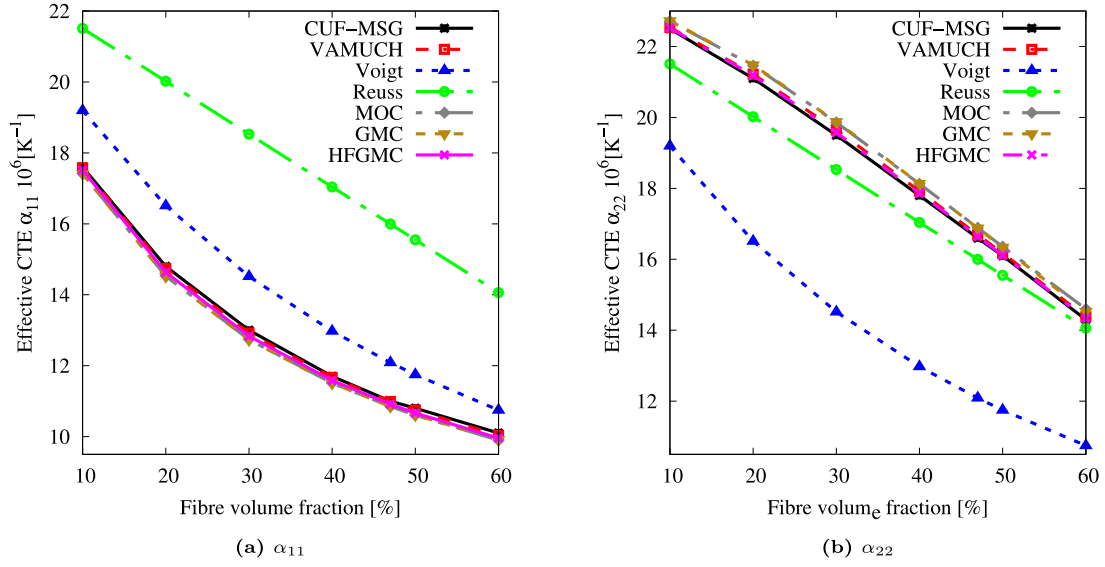$$

**Fig. 5.** Variation of the CTEs of fibre-reinforced composite B/Al square-pack with regard to the percentage fibre volume fraction. An HLE of eighth order is used as expansion function in these plots.
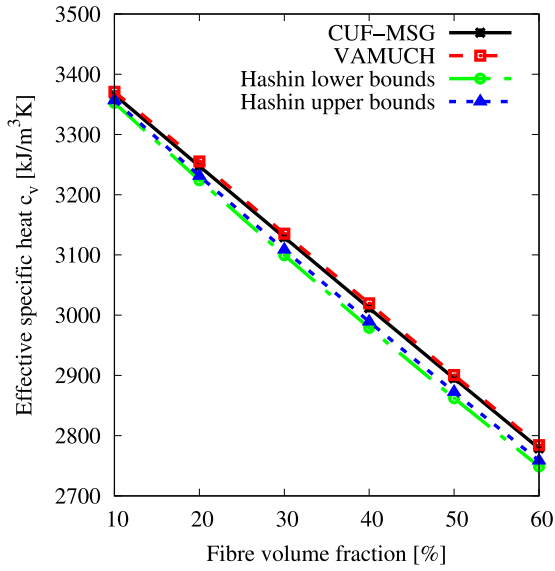


**Fig. 6.** Variation of the effective specific heat $c_v$ of fibre-reinforced SiC/Cu square-pack with regard to the percentage of fibre volume fraction. An HLE of eighth order is used as expansion function in this plot.
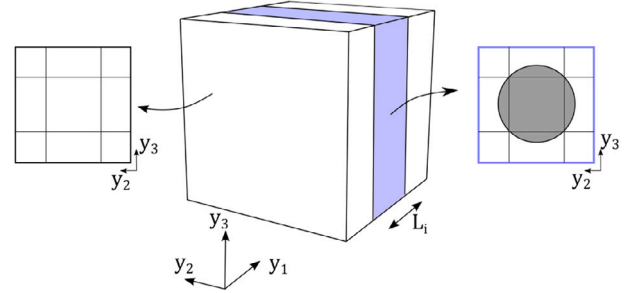


**Fig. 7.** HLE beam model of cylindrical particle-reinforced RUC. $L_i$ denotes the length of the inclusion along which the mapped circular expansion is used.

form of $\mathbf{D}_{h\theta}^{\tau i}$ is:

$$
\begin{aligned}
\boldsymbol{D}_{h\theta 11}^{\tau i} &= \beta_{11} \int_l N_{i,y_1} dy_1 \int_\Omega F_\tau d\Omega + \beta_{13} \int_l N_i dy_1 \int_\Omega F_{\tau,y_3} d\Omega \\
&\quad + \beta_{12} \int_l N_i dy_1 \int_\Omega F_{\tau,y_2} d\Omega
\end{aligned}
$$

$$
\begin{aligned}
\boldsymbol{D}_{h\theta 21}^{\tau i} &= \beta_{22} \int_l N_i dy_1 \int_\Omega F_{\tau,y_2} d\Omega + \beta_{23} \int_l N_i dy_1 \int_\Omega F_{\tau,y_3} d\Omega \\
&\quad + \beta_{12} \int_l N_{i,y_1} dy_1 \int_\Omega F_\tau d\Omega
\end{aligned} \tag{22}
$$

$$
\begin{aligned}
\boldsymbol{D}_{h\theta 31}^{\tau i} &= \beta_{33} \int_l N_i dy_1 \int_\Omega F_{\tau,y_3} d\Omega + \beta_{23} \int_l N_i dy_1 \int_\Omega F_{\tau,y_2} d\Omega \\
&\quad + \beta_{12} \int_l N_{i,y_1} dy_1 \int_\Omega F_\tau d\Omega
\end{aligned}
$$

The fluctuation unknowns that minimise the functional in Eq. (20) can be retrieved by solving the following linear system:

$$
\mathbf{E}\chi = -\mathbf{D}_{h\varepsilon}\bar{\varepsilon} - \mathbf{D}_{h\theta}\theta \tag{23}
$$

Then, assuming the fluctuation is linearly proportional to $\bar{\varepsilon}$ and $\theta$, i.e.:

$$
\chi = \chi_0 \bar{\varepsilon} + \chi_\theta \theta \tag{24}
$$

and substituting it into Eq. (23), one can write the following linear system:

$$
\begin{cases} \mathbf{E}\chi_0 = -\mathbf{D}_{h\varepsilon} \\ \mathbf{E}\chi_\theta = -\mathbf{D}_{h\theta} \end{cases} \tag{25}
$$

where $\chi_0$ and $\chi_\theta$ are respectively $3 \times 6$ and $3 \times 1$ matrices.

being $\mathbf{I}$ the $3 \times 3$ identity array. On the one hand, the $3 \times 3$ $\mathbf{E}^{\tau sij}$ matrix, the $3 \times 6$ $\mathbf{D}_{h\varepsilon}^{sj}$ matrix, and the $3 \times 1$ $\mathbf{D}_{h\theta}^{sj}$ matrix are the fundamental nuclei of the thermo-elastic RUC structural problem, which contain the complete details about the structural problem. Furthermore, $\mathbf{D}_{\varepsilon\varepsilon}$, $\mathbf{D}_{\varepsilon\theta}$ and $D_{\theta\theta}$ are the averaged stiffness matrix, averaged thermal stiffness matrix and averaged specific heat of the material, respectively. Consequently, looping through the indexes $\tau sij$, one can calculate the assembled $\mathbf{E}$, $\mathbf{D}_{h\varepsilon}$ and $\mathbf{D}_{h\theta}$ matrices for the RUC problem. The indices $\tau$ and $s$ constitute the loop over the cross-sectional functions, depending on the $F_\tau$ selected and the number of expansions terms assumed. Whereas the loop on the $i$ and $j$ subscripts depends on the chosen shape functions. For the sake of brevity, the extended-expression of the matrices $\mathbf{E}^{\tau sij}$ and $\mathbf{D}_{h\varepsilon}^{\tau i}$ are not given in this article. However, these can be consulted in the work of de Miguel et al. [7], whereas the explicit
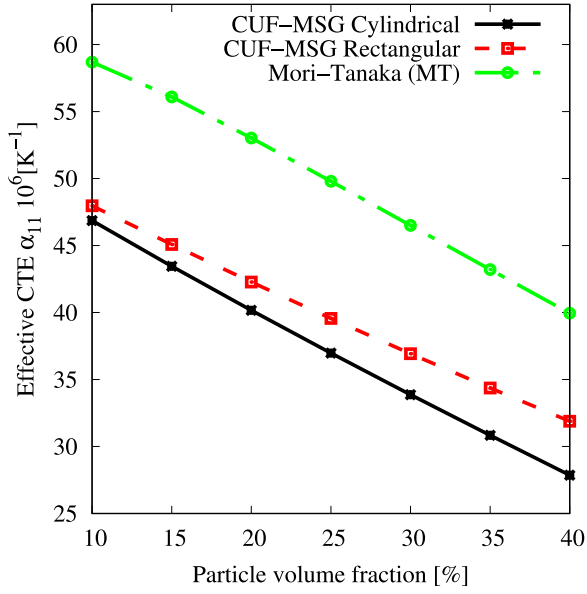
**Fig. 8.** Variation of the effective CTE of a particle-reinforced composite glass/epoxy with regard to the percentage of inclusion volume fraction. An HLE of eighth order is used as expansion function in this plot.



**Fig. 9.** Variation of the effective specific heat $c_v$ of particle-reinforced composite steel/Al with regard to the percentage of inclusion volume fraction. An HLE of eighth order is used as expansion function in this plot.

Finally, substituting Eq. (24) in the functional from Eq. (19), one can calculate

$$\Pi^* = \frac{1}{2}\bar{\varepsilon}^T \mathbf{C}^* \bar{\varepsilon} + \bar{\varepsilon}^T \bar{\beta}\theta + \frac{1}{2}\bar{c}_v \frac{\theta^2}{T_0} \tag{26}$$

with

$$\mathbf{C}^* = \frac{1}{\Omega}(\chi_0^T \mathbf{D}_{h\varepsilon} + \mathbf{D}_{\varepsilon\varepsilon})\bar{\beta} = \frac{1}{\Omega}\left[\frac{1}{2}(\mathbf{D}_{h\varepsilon}^T \chi_\theta + \chi_0^T \mathbf{D}_{h\theta}) + \mathbf{D}_{\varepsilon\theta}\right] \tag{27}$$

$$\bar{c}_v = \frac{1}{\Omega}[\chi_\theta^T \mathbf{D}_{h\theta} T_0 + \mathbf{D}_{\theta\theta}]$$

where $\bar{\varepsilon}$ represents the global strains, $\mathbf{C}^*$ is the effective elastic coefficients matrix of the equivalent material, $\bar{\beta}$ is the effective thermal stress coefficients vector and lastly, $\bar{c}_v$ is the effective specific heat. Besides, $\mathbf{D}_{h\varepsilon}$, $\mathbf{D}_{\varepsilon\varepsilon}$, $\mathbf{D}_{h\theta}$, $\mathbf{D}_{\varepsilon\theta}$ and $\mathbf{D}_{\theta\theta}$ are the assembled arrays of their aforementioned fundamental nuclei. It is clear that through the following expression, the effective coefficients of the thermal expansion can be obtained:

$$\bar{\alpha} = -\mathbf{C}^{*-1}\bar{\beta} \tag{28}$$

Now, by reintroducing the fluctuation solutions into the geometrical and constitutive expressions, the local fields over the RUC can be directly derived. The real solution to the fluctuation function is:

$$\chi = \chi_0 \bar{\varepsilon} + \chi_\theta \theta \tag{29}$$

Consequently, the local strains become:

$$\varepsilon = \bar{\varepsilon} + \mathbf{D}(F_\tau N_i \chi) \tag{30}$$

Ultimately, using Hooke's law, one can recover the local stresses of the initial heterogeneous material.

$$\sigma = \mathbf{C}\varepsilon + \beta\theta \tag{31}$$

## 4. Numerical results

The numerical results reported in this manuscript aim to validate the given formulation and demonstrate the accuracy of the HLE beam model for the precise thermo-elastic analysis of the RUC model. First,
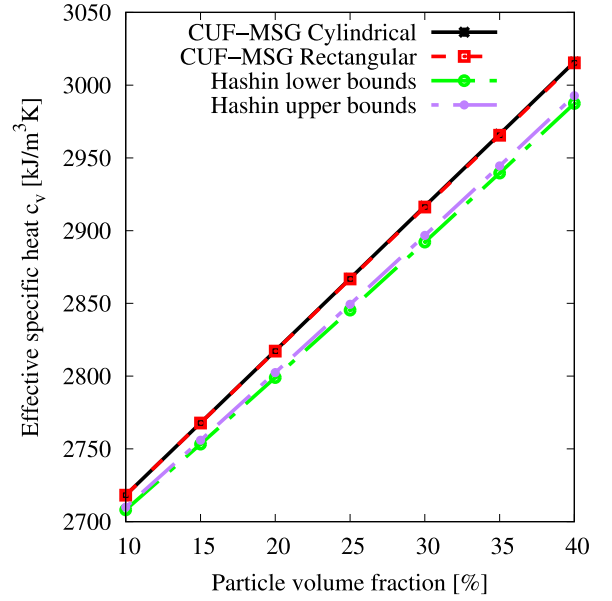
reference problems concerning fibre- and particle-reinforced composites are addressed, and thermal properties are compared with those found in the literature.

Subsequently, the effectiveness of the 1D approach and MSG formulation is proven for both the homogenisation and the stress recover problem by comparing against already established software tools such as SwiftComp [29], that also exploits MSG. The difference between the present approach and SwiftComp resides in the fact that MSG-CUF approach uses beam finite elements along the longitudinal direction of the reinforcement and 2D elements for the cross-section. Conversely, SwiftComp utilises 2D FE in the case of fibre reinforced RUC, whereas 3D elements are employed when particles are involved.

### 4.1. Fibre-reinforced unit cell

The first analysis comprises a boron fibre embedded in an aluminum matrix, denoted as B/Al hereinafter, arranged in a square-pack geometry, see Fig. 4. Due to the arrangement of the fibre into the RUC, the fluctuation unknowns will be invariants along the fibre direction. For that reason, in such cases, a single linear beam element (B2) is sufficient to interpolate unknowns along the beam axis. It is clear that the solution does not change when the order of the beam element is increased.

The two constituents are isotropic, with $E = 379.3$ GPa, $\nu = 0.10$ and $\alpha = 8.1 \cdot 10^{-6}$ K$^{-1}$ for boron fibres, whilst $E = 68.3$ GPa, $\nu = 0.30$ and $\alpha = 23.0 \cdot 10^{-6}$ K$^{-1}$ for the aluminum matrix. A comparison between the results provided by the different HLE order and existing literature is available in Table 1. In there, the volume fraction of the fibre is set to 0.47. The reference results are based on both analytical formulae (Rosen and Hashin [9], Voigt [35] and Reuss [36]) and numerical methods (MOC [13], GMC [14], HFGMC [15] and Tamma and Avila [37]). It is appreciated that the results show a high level of agreement between the proposed methodology and the reference results, with the exception of Voigt and Reuss, which are variations to the rule of mixtures.

Furthermore, the variation of the longitudinal and transverse CTEs related to the volume fraction is included in Fig. 5. The beam theory considered an HLE expansion of eight order to conduct this comparison.
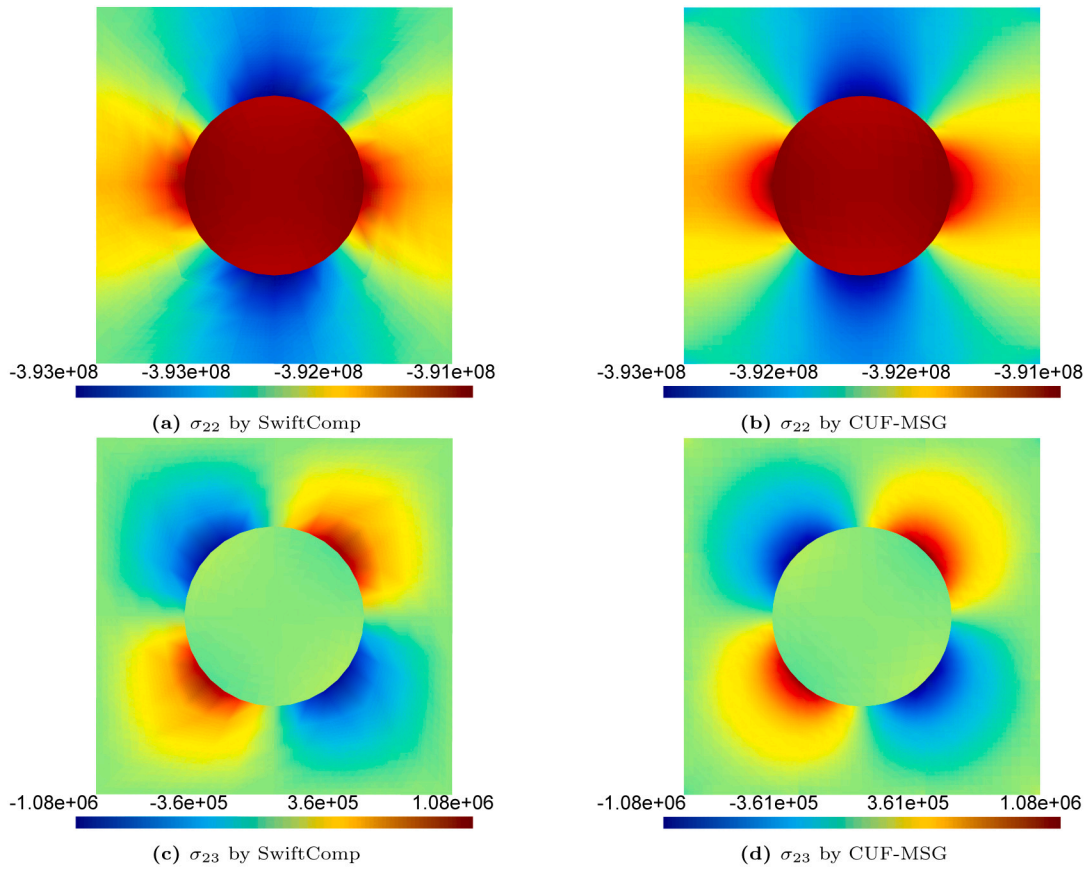
**(a)** $\sigma_{22}$ by SwiftComp

-3.93e+08    -3.93e+08    -3.92e+08    -3.91e+08

**(b)** $\sigma_{22}$ by CUF-MSG

-3.93e+08    -3.92e+08    -3.92e+08    -3.91e+08

**(c)** $\sigma_{23}$ by SwiftComp

-1.08e+06    -3.6e+05    3.6e+05    1.08e+06

**(d)** $\sigma_{23}$ by CUF-MSG

-1.08e+06    -3.61e+05    3.61e+05    1.08e+06

**Fig. 10.** Stress state due to a rise in temperature equal to $\theta = 100$ K of a B/Al square-pack. Stresses are reported in Pa.

**Table 1**
Effective CTEs of fibre-reinforced composite B/Al square-pack provided by the literature and the present approach, considering different HLE polynomial order. The fibre volume fraction is set to 0.47.

| Model | DOF | $\alpha_{11} \cdot 10^6$ [K$^{-1}$] | $\alpha_{22} \cdot 10^6$ [K$^{-1}$] |
|---|---|---|---|
| Reference solutions | | | |
| Rosen and Hashin [9] | – | 10.99 | 16.69 |
| VAMUCH [29] | – | 10.99 | 16.69 |
| Voigt [35] | – | 12.09 | 12.09 |
| Reuss [36] | – | 16.00 | 16.00 |
| MOC [13] | – | 10.85 | 16.89 |
| GMC [14] | – | 10.85 | 16.88 |
| HFGMC [15] | – | 10.91 | 16.34 |
| Tamma and Avila [37] | – | 10.77 | 17.34 |
| CUF-MSG | | | |
| HLE 2 | 240 | 11.06 | 16.48 |
| HLE 4 | 582 | 11.02 | 16.59 |
| HLE 6 | 1140 | 11.02 | 16.60 |
| HLE 8 | 1914 | 11.02 | 16.61 |

Again, it is appreciated a perfect match between CUF-MSG and the numerical solutions from the literature, whilst more significant differences are found when compared to analytical solutions (Voigt [35], and Reuss [36]), through all the fibre volume range.

The second assessment aims to predict the effective specific heat of macroscopically anisotropic composites, such as the one conformed by a silicon carbide fibre embedded in a copper matrix, referred to as SiC/Cu composite. These two constituents are considered as isotropic with $E = 410$ GPa, $v = 0.14$, $\alpha = 4.0 \cdot 10^{-6}$ K$^{-1}$, and $c_v = 2327.73$ kJ/(m$^3$ K) for SiC fibres, and $E = 117$ GPa, $v = 0.34$, $\alpha = 22.0 \cdot 10^{-6}$ K$^{-1}$, and $c_v = 3485.09$ kJ/(m$^3$ K) for the copper matrix. The variation of the specific heat when the volume fraction of the SiC fibre varies is plotted

in Fig. 6. Once again, good agreement between the solutions proposed by Rosen and Hashin [9], VAMUCH [20] and CUF-MSG is found.

### 4.2. Particle-reinforced unit cell

The aim of this section is to investigate the influence that the geometry of the reinforcement particles has on the thermal properties of the composites. For doing so, two kinds of inclusions are considered: rectangular and cylindrical. The latter is represented in Fig. 7. When dealing with these cases, the constituents vary over the three spatial directions of the RUC. Therefore, in order to capture the correct description of the changes along the beam axis, the present numerical results employed six four-node cubic beam elements (B4). The different phases are involved in the numerical model thanks to the CW capabilities of CUF. A glass/epoxy reinforced composite is analysed first. The glass properties are set to $E = 72.38$ GPa, $v = 0.20$ and $\alpha = 5.0 \cdot 10^{-6}$ K$^{-1}$, whereas the epoxy matrix presents $E = 2.75$ GPa, $v = 0.35$, $\alpha = 54.0 \cdot 10^{-6}$ K$^{-1}$.

The outcomes provided by both of the inclusion types are confronted with the Mori–Tanaka (MT) method [12], which is widely used for reinforced materials, regardless of the geometry of the reinforcing constituent. Results are reported in Fig. 8. It is inferred that the difference between cylindrical and rectangular inclusion for low particle volume fraction could be neglected, whereas greater discrepancies appear for larger particle fraction. Moreover, it is appreciated that both geometries predict different effective CTEs when compared to MT, which overestimates its value.

An additional comparison for the calculation of the homogenised thermo-elastic properties is made by comparing the already mentioned geometries against a spherical inclusion, modelled in SwiftComp. The outcomes are gathered in Table 2. Note that the longitudinal CTE $\alpha_{11}$
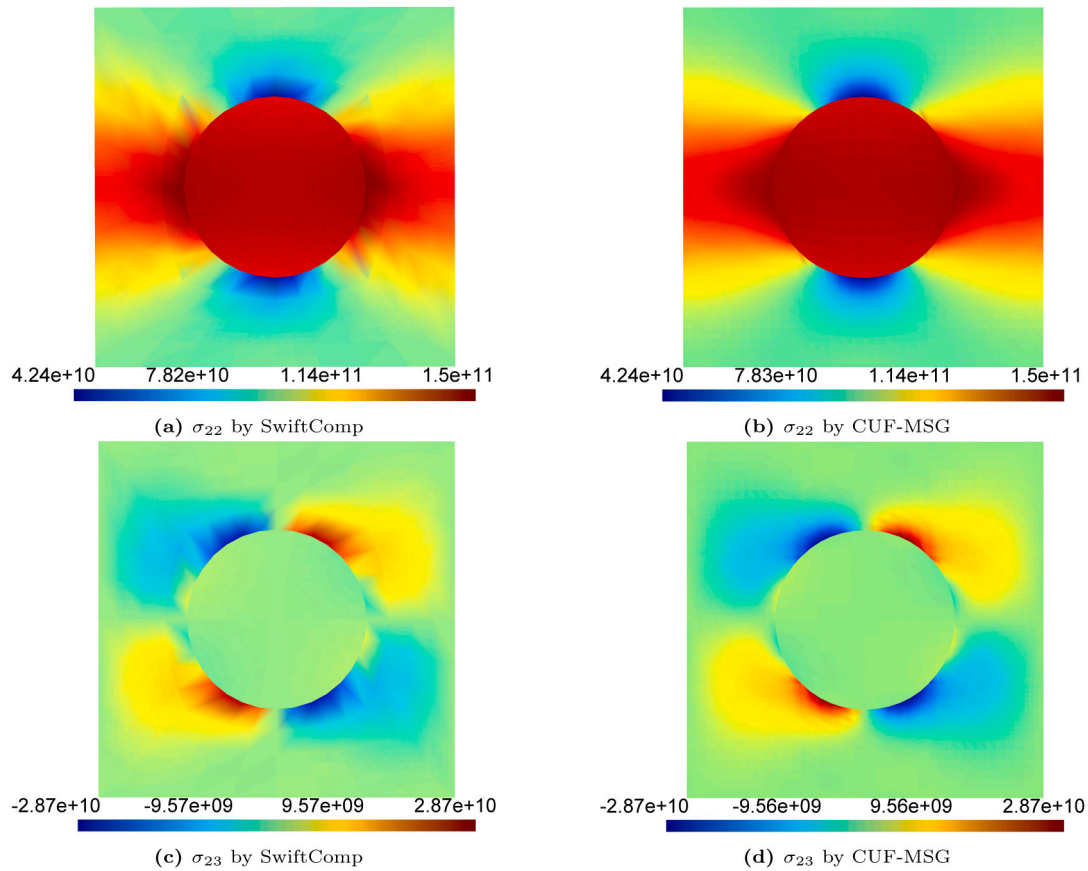
**(a)** $\sigma_{22}$ by SwiftComp



**(b)** $\sigma_{22}$ by CUF-MSG



**(c)** $\sigma_{23}$ by SwiftComp



**(d)** $\sigma_{23}$ by CUF-MSG

**Fig. 11.** Stress state due to a rise in temperature equal to $\theta = 100$ K and a unitary longitudinal strain $\varepsilon_{11}$ of a B/Al square-pack. Stresses are reported in Pa.
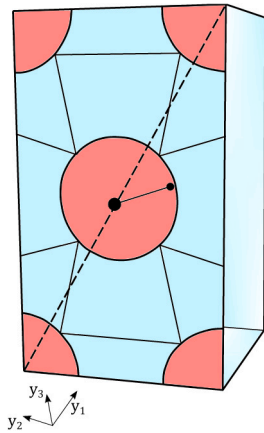


**Fig. 12.** HLE beam model of a hexa-pack RUC.

**Table 2**
Effective CTEs of particle-reinforced composite glass/epoxy provided by the literature and the present approach, considering different HLE polynomial order and inclusion geometry. The particle volume fraction is set to 0.3.

| Model | Expansion theory | $\alpha_{11} \cdot 10^6$ [K$^{-1}$] | $\alpha_{22} \cdot 10^6$ [K$^{-1}$] |
|---|---|---|---|
| VAMUCH spherical [29] | – | 35.50 | 34.97 |
| Mori–Tanaka (MT)[12] | – | 46.50 | 9.31 |
| CUF-MSG cylindrical | HLE 3 | 33.79 | 38.73 |
|  | HLE 6 | 33.86 | 38.78 |
|  | HLE 8 | 33.87 | 38.78 |
| CUF-MSG rectangular | HLE 3 | 36.85 | 36.80 |
|  | HLE 6 | 36.93 | 36.89 |
|  | HLE 8 | 36.93 | 36.90 |

parallelepiped inclusion, as opposed for the previous inclusion analysis. Slight differences are appreciated compared to Rosen and Hashin [9] analytical approach.

### 4.3. Prediction of local stresses

A more complex procedure is the recovery of local stresses between matrix and fibre at the RUC level when a load is applied to the global structure. High gradients in strain/stress solutions require highly refined models. In the case of refined beam elements, particularly HLE modelling, high-order polynomials are needed to provide accurate solutions.

The last numerical comprises the prediction of the local stresses generated by unitary strains and thermal loading. In the first example, a B/Al square-pack is compared against SwiftComp [29] outcomes for the same loading conditions. The fibre volume fraction selected is 0.20. First, the temperature is increased by 100 K with a strain-free condition.

of the spherical inclusion lies between those of the cylindrical and rectangular inclusions. Conversely, the transverse CTE $\alpha_{22}$ of the spherical inclusion is lower than those provided by the CUF-MSG models.

An aluminum matrix is strengthened with steel inclusions for the last example concerning the computation of the effective specific heat of particle-reinforced composites. Both constituents are modelled as isotropic. The steel fibre are assumed to be $E = 200$ GPa, $\nu = 0.30$ and $\alpha = 12.0 \cdot 10^{-6}$ K$^{-1}$ and $c_\nu = 3609.6$ kJ/(m$^3$ K), whilst the Aluminum thermo-elastic properties of the matrix are $E = 68.3$ GPa, $\nu = 0.330$, $\alpha = 23.0 \cdot 10^{-6}$ K$^{-1}$ and $c_\nu = 2619.1$ kJ/(m$^3$ K). The effective $c_\nu$ predicted for different values of the particle fraction are represented in Fig. 9. It is noteworthy that no difference is found between the cylindrical and

**(a)** $\sigma_{22}$ by CUF-MSG



**(b)** $\sigma_{22}$ distribution



**(c)** $\sigma_{23}$ by CUF-MSG



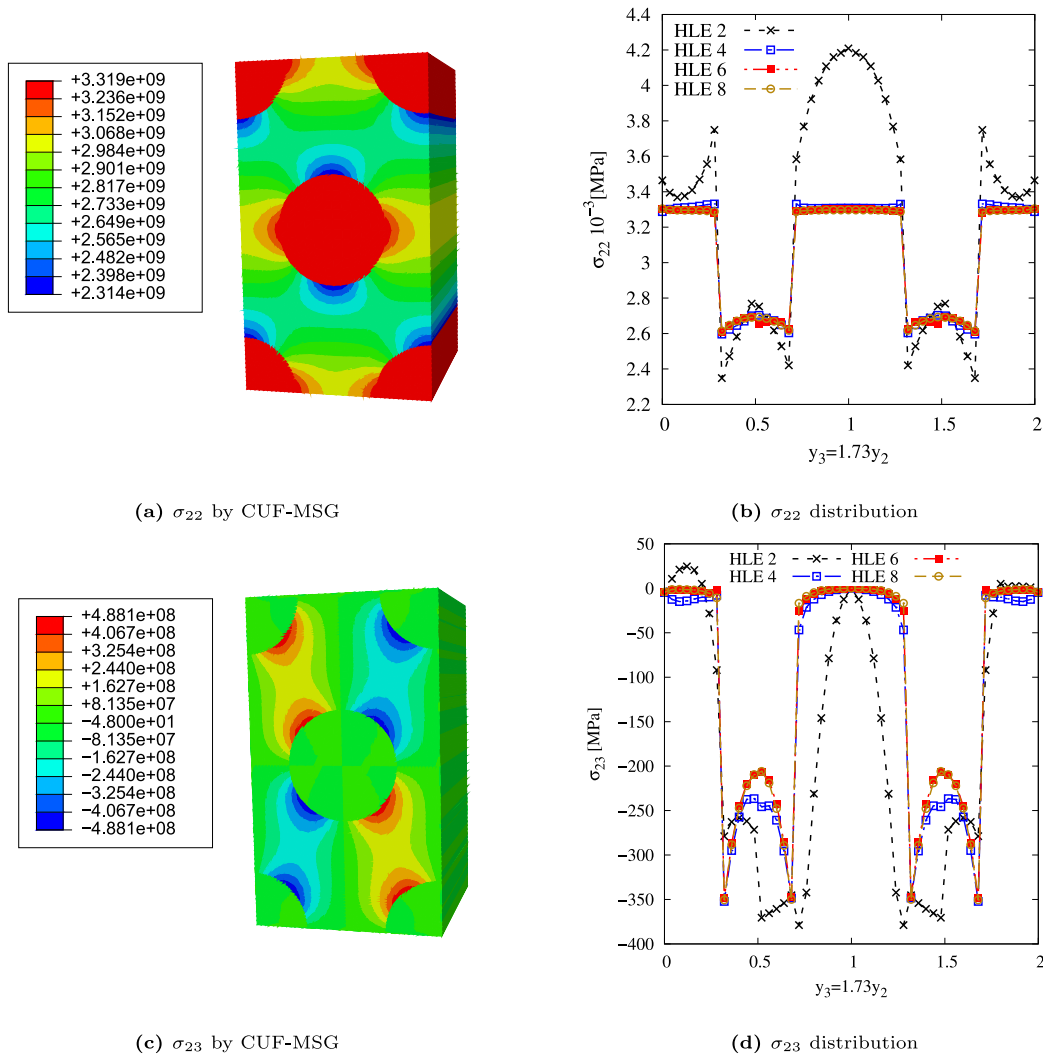**(d)** $\sigma_{23}$ distribution

**Fig. 13.** Stress state due to a rise in temperature equal to $\theta = 100$ K and a unitary longitudinal strain $\varepsilon_{11}$ of a glass/epoxy hexa-pack. An HLE of eight order is used as expansion in the 3D representation.

Then, a unitary longitudinal strain ($\varepsilon_{11} = 1$) is applied in addition to the previous temperature rise. Results are depicted in Figs. 10 and 11, respectively. The left-hand side of those figures provides the SwiftComp outcomes, whereas those obtained by the present approach are available on the right-hand side.

Fig. 10 illustrates the stress state only due to a rise in temperature. Because of the discrepancy between the constituents' CTEs, thermal stresses arise. It is observed that the transverse stress component has a compressive character. Concerning the transverse shear, the doubly antisymmetric stress distribution is retrieved. Additionally, a good agreement between SwiftComp and CUF-MSG is found. Indeed, only a 0.06 MPa difference is observed when computing $\sigma_{23}$. On the other hand, when a unitary longitudinal strain is also accounted for, the stresses are generated because of the differences in the elastic properties of the components. As expected, higher stresses are appreciated. In this case, $\sigma_{22}$ corresponds to traction stresses due to the pulling in the longitudinal direction. Therein, it is the boron fibre the one presenting the higher stresses as expected. Relative to $\sigma_{23}$, a similar distribution to that of Fig. 10(d) is obtained. Again, a good agreement between SwiftComp and CUF-MSG is appreciated, even if greater discrepancies are found in comparison to the previous numerical results.

As a final result, the local stress state of a glass/epoxy hexa-pack is shown hereinafter. The glass fibre is modelled as isotropic with $E = 72.38$ GPa, $v = 0.20$ and $\alpha = 5.0 \cdot 10^{-6}$ K$^{-1}$, whilst the epoxy matrix is also

considered isotropic with $E = 2.75$ GPa, $v = 0.35$ and $\alpha = 55.0 \cdot 10^{-6}$ K$^{-1}$. The fibre volume fraction selected is 0.30. In Fig. 12 is displayed the HLE beam model for the hexa-pack. The cross-section comprises fifteen expansion subdomains, in which five correspond to the fibres and the remaining ten to the matrix. For this numerical case, highly refined micromechanics models need to be employed to capture strain/stress solutions with high gradients. For such purpose, if the aim is to capture the local solutions with an accuracy similar to that of 3D FEM, high-order HLE beam models need to be used. Hence, HLE 8 expansions are utilised. Fig. 13 shows the longitudinal $\sigma_{11}$ and transverse $\sigma_{13}$ local stresses generated by setting longitudinal strain $\varepsilon_{11}$ equal to 1 and a 100 K raise in temperature. Likewise, Figs. 13(b) and 13(d) show the variation of $\sigma_{22}$ and $\sigma_{23}$ along the diagonal represented in Fig. 12. As stated before, high-order HLE expansions allow capturing the high-stress gradients that occur at the fibre–matrix interface, as shown in the figures mentioned above. This is better appreciated for the transverse stresses where the fibre and matrix, respectively, produce tension and compression stresses.

## 5. Conclusions

This work has presented the introduction of an advanced beam modelling approach to solve micromechanical thermo-elastic analyses. These models made use of 1D elements to characterise the fibre, or

reinforcement, direction, whilst the fibres' arrangement is represented in the cross-section of the one-dimensional elements. MSG is used to uncouple the multiscale problem and subdivide it into a local and global analysis. In this manner, the effective thermal properties (CTEs and specific heat), along with the purely mechanical, for heterogeneous materials and the local stress distribution can be computed in one single run of the code.

The present methodology relies on a non-isoparametric mapping technique using HLE 1D models, which permits generating perfect curved edges in the model without increasing the computational burden of the numerical model. Indeed, the computational cost is only increased depending on the order of the HLE polynomials, which represents an input of the analysis.

The model's validity has been demonstrated via comparison with the MSG-based programme SwiftComp, as well as reference solutions that rely on both analytical and/or semi-analytical approaches, such as Voigt, Reuss, Mori–Tanaka, MOC and HFGMC, among others. The presented research dealt only with linear thermo-elastic cases and classic RUC geometries. However, its extension to heat conduction, hygro-thermal diffusivity and multiscale analysis shall be pursued in future developments.

## CRediT authorship contribution statement

**A.R. Sánchez-Majano:** Software, Validation, Writing – original draft, Visualization. **R. Masia:** Software, Validation, Writing – original draft, Visualization. **A. Pagani:** Conceptualization, Methodology, Writing – review & editing, Supervision, Project administration, Funding acquisition. **E. Carrera:** Conceptualization, Methodology.

## Declaration of competing interest

The authors declare that they have no known competing financial interests or personal relationships that could have appeared to influence the work reported in this paper.

## Data availability

Data will be made available on request.

## Acknowledgements

## References

[1] Llorca J, González C, Molina-Aldareguía JM, Segurado J, Seltzer R, Sket F, Rodríguez M, Sádaba S, Muñoz R, Canal LP. Multiscale modeling of composite materials: a roadmap towards virtual testing. Adv Mater 2011;23(44):5130–47.

[2] Huang Y, Xu L, Kyu Ha S. Prediction of three-dimensional composite laminate response using micromechanics of failure. J Compos Mater 2012;46(19–20):2431–42.

[3] Pineda EJ, Bednarcyk BA, Waas AM, Arnold SM. Progressive failure of a unidirectional fiber-reinforced composite using the method of cells: Discretization objective computational results. Int J Solids Struct 2013;50(9):1203–16.

[4] Hassani B, Hinton E. A review of homogenization and topology optimization I—homogenization theory for media with periodic structure. Comput Struct 1998;69(6):707–17.

[5] Nemat-Nasser S, Hori M. Micromechanics: overall properties of heterogeneous materials. 2013.

[6] Aboudi J, Arnold SM, Bednarcyk BA. Practical micromechanics of composite materials. 2021.

[7] de Miguel AG, Pagani A, Yu W, Carrera E. Micromechanics of periodically heterogeneous materials using higher-order beam theories and the mechanics of structure genome. Compos Struct 2017;180.

[8] Hill R. The elastic behaviour of a crystalline aggregate. Proc Phys Soc. Sec A 1952;65(5):349.

[9] Rosen BW, Hashin Z. Effective thermal expansion coefficients and specific heats of composite materials. Internat J Engrg Sci 1970;8(2):157–73.

[10] Hashin Z, Shtrikman S. A variational approach to the theory of the elastic behaviour of polycrystals. J Mech Phys Solids 1962;10(4):343–52.

[11] Williams TO. A three-dimensional, higher-order, elasticity-based micromechanics model. Int J Solids Struct 2005;42(3–4):971–1007.

[12] Mori T, Tanaka K. Average stress in matrix and average elastic energy of materials with misfitting inclusions. Acta Metall 1973;21(5):571–4.

[13] Aboudi J. A continuum theory for fiber-reinforced elastic-viscoplastic composites. Internat J Engrg Sci 1982;20(5):605–21.

[14] Paley M, Aboudi J. Micromechanical analysis of composites by the generalized cells model. Mech Mater 1992;14(2):127–39.

[15] Aboudi J, Pineda MJ, Arnold SM. Linear thermoelastic higher-order theory for periodic multiphase materials. J Appl Mech 2001;68(5):697–707.

[16] Sun CT, Vaidya RS. Prediction of composite properties from a representative volume element. Compos Sci Technol 1996;56(2):171–9.

[17] Sahu P, Sharma N, Dewangan H, Panda S. Theoretical prediction and experimental validity of thermal frequency responses of laminated advanced fiber-reinforced epoxy hybrid composite panel. Int J Struct Stab Dyn 2022.

[18] Yu W. A unified theory for constitutive modeling of composites. J Mech Mater Struct 2016;379–411.

[19] Yu W, Hodges DH, Ho JC. Variational asymptotic beam sectional analysis - An updated version. Internat J Engrg Sci 2012;59:40–64.

[20] Yu W, Tang T. A variational asymptotic micromechanics model for predicting thermoelastic properties of heterogeneous materials. Int J Solids Struct 2007;44(22):7510–25.

[21] Liu X, Peng B, Yu W. Multiscale modeling of the effective thermal conductivity of 2D woven composites by mechanics of structure genome and neural networks. Int J Heat Mass Transfer 2021;179:121673.

[22] Carrera E, Cinefra M, Petrolo M, Zappino E. Finite element analysis of structures through unified formulation. Hoboken, New Jersey, USA; 2014.

[23] Azzara R, Carrera E, Filippi M, Pagani A. Time response stress analysis of solid and reinforced thin-walled structures by component-wise models. Int J Struct Stab Dyn 2020;20(14):2043010.

[24] Pagani A, Enea M, Carrera E. Quasi-static fracture analysis by coupled three-dimensional peridynamics and high order one-dimensional finite elements based on local elasticity. Internat J Numer Methods Engrg 2021.

[25] Sánchez-Majano AR, Azzara R, Pagani A, Carrera E. Accurate stress analysis of variable angle tow shells by high-order equivalent-single-layer and layer-wise finite element models. Materials 2021;14(21):6486.

[26] Azzara R, Carrera E, Pagani A. Nonlinear and linearized vibration analysis of plates and shells subjected to compressive loading. Int J Non-Linear Mech 2022;103936.

[27] Carrera E, de Miguel AG, Pagani A. Hierarchical theories of structures based on Legendre polynomial expansions with finite element applications. Int J Mech Sci 2017;120:286–300.

[28] Pagani A, de Miguel AG, Carrera E. Cross-sectional mapping for refined beam elements with applications to shell-like structures. Comput Mech 2017;59(6):1031–48.

[29] Yu W, Liu X. Swiftcomp. 2017.

[30] Carrera E, Pagani A, Augello R. Large deflection of composite beams by finite elements with node-dependent kinematics. Comput Mech 2022.

[31] Pagani A, Azzara R, Augello R, Carrera E, Wu B. Accurate through-the-thickness stress distributions in thin-walled metallic structures subjected to large displacements and large rotations. Vietnam J Mech 2020;42:239–54.

[32] Szabó B, Düster A, Rank E. The p-version of the finite element method. In: Encyclopedia of computational mechanics. 2004.

[33] Carrera E, Pagani A, Petrolo M. Classical, refined, and component-wise analysis of reinforced-shell wing structures. AIAA J 2013;51(5):1255–68.

[34] Gordon WJ, Hall CA. Transfinite element methods: Blending-function interpolation over arbitrary curved element domains. Numer Math 1973;21:109–29.

[35] Voigt W. Theoretische studien über die elasticitätsverhältnisse der krystalle. Abh D Königlichen Gesellschaft D Wissensch Göttingen 1887;34:3–51.

[36] Reuß A. Berechnung der fließgrenze von mischkristallen auf grund der plastizitätsbedingung für einkristalle.. ZAMM Z. Angew. Math. Mech 1929;9(1):49–58.

[37] Tamma KK, Avila AF. An integrated micro/macro modeling and computational methodology for high temperature composites. Rochester, NY.; 1999, p. 143–256.